

MODELING THE AFTERGLOW OF GW150914-GBM

BRIAN J. MORSONY¹

Dept. of Astronomy, University of Maryland, 1113 Physical Sciences Complex, College Park, MD, 20742-2421, USA

JARED C. WORKMAN

Dept. of Physical and Environmental Sciences, Colorado Mesa University, Grand Junction, CO, 81501, USA

DOMINIC M. RYAN

Dept. of Astronomy, University of California, Berkeley, 501 Campbell Hall #3411, Berkeley, CA, 94720-4311, USA

¹morsony@astro.umd.edu

ABSTRACT

We model the possible afterglow of the *Fermi* GBM event associated with LIGO detection GW150914, under the assumption that the gamma-ray are produced by a short GRB-like relativistic outflow. We model GW150914-GBM as both a weak, on-axis short GRB and normal short GRB seen far off axis. Given the large uncertainty in the position of GW150914, we determine that the best chance of finding the afterglow is with the MWA or ASKAP, with the flux from an off-axis short GRB reaching 0.3 - 10 mJy (0.17 - 42 mJy) at 150 MHz (863.5 MHz) by 1 - 12 months after the initial event. At low frequencies, the source would evolve from a hard to soft spectrum over several months. The radio afterglow would be detectable for several months to years after it peaks, meaning the afterglow may still be detectable and increasing in brightness **NOW** (mid Feb. 2016). With a localization from the MWA or ASKAP, the afterglow would be detectable at higher radio frequencies with the ATCA and in X-rays with *Chandra* or XMM.

Keywords: gravitational waves — gamma-ray bursts: individual: GW150914-GBM — gamma-ray bursts: general

1. INTRODUCTION

GW150914 is the first gravitational wave source detected by LIGO (Abbott et al. 2016a), and is the merger of two approximately $30 M_{\odot}$ black holes. The merger occurred at a distance of 410^{+160}_{-180} Mpc ($z = 0.09^{+0.03}_{-0.04}$) in the southern hemisphere (Abbott et al. 2016a). Although the merger of two large black holes was not expected to produce a bright electromagnetic signature (Connaughton et al. 2016), the *Fermi* Gamma-ray Burst Monitor (GBM) found a 1 second increase in gamma-ray emission 0.4 seconds after the LIGO detection, and located in the same region of the sky (Connaughton et al. 2016). INTEGRAL did not detect an event associated with GW150914 (Savchenko et al. 2016), in tension with the GBM results.

Assuming the GBM detection is associated with GW150914, it would have an isotropic luminosity of $E_{iso} = 1.8^{+1.5}_{-1.0} \times 10^{49}$ erg, an order of magnitude fainter than any other short-GRB analyzed

(Connaughton et al. 2016; Wanderman & Piran 2015). Typical short GRB energies range from $E_{iso} = 10^{50} - 10^{52}$ (Fong et al. 2015). The properties of the *Fermi* GBM detection are broadly consistent with a short GRB, although it would be significantly harder than the typical E_{peak} - E_{iso} relation for short GRBs (Li et al. 2016). It is possible that GW150914 produced either an under-luminous short-GRB, a poorly collimated jet, or that it is a typical short GRB but seen far off-axis, so that the prompt emission directed towards Earth was faint.

GW150914 occurred in the southern hemisphere, but was poorly localized, with the combined LIGO and *Fermi* GBM error boxes covering 199 deg^2 (Connaughton et al. 2016). This made it very difficult to localized the early, rapidly fading X-ray or optical afterglow. Non-detections have been reported by *Swift* XRT and UVOT (Evans et al. 2016), the Dark Energy Camera (Soares-Santos et al. 2016), and Pan-STARRS

and PESSTO (Smartt et al. 2016).

In the radio, a GRBs afterglow produces a persistent source, but is initially self-absorbed, taking weeks to months to reach peak luminosity. The best prospect for finding the afterglow would be with a wide-field instrument, such as the Murchinson Widefield Array (MWA) , a low-frequency (80 - 300 MHz) radio array (Tingay et al. 2013), or the ASKAP Boolardy Engineering Test Array (BETA) at 713.5 - 1013.5 MHz (Hobbs et al. 2016), both located in Australia. MWA is sensitive to sources brighter than about ~ 6 mJy before becoming confusion limited at 150 MHz (Tingay et al. 2013), and ASKAP is currently sensitive down to ~ 3 mJy at 862.5 MHz (GCN 18363). The Australia Compact Telescope Array (ATCA), at 1.1 - 3.1 GHz, is sensitive to much fainter sources (0.04mJy in 10 minute integration), but has a much smaller field of view (0.4 to 0.05 deg 2 vs. 600 deg 2 for MWA and 30 deg 2 for ASKAP), making covering the large possible area for GW150914 difficult. It would, however, be able to follow up any candidate afterglow sources.

The best way to determine if LIGO event GW150914 and the *Fermi* GBM detection are associated would be to find an afterglow that can be localized to a host galaxy.

We model the possible afterglow of GW150914-GBM as a relativistic blastwave expanding into the surrounding medium, and emitting synchrotron radiation. For a review of afterglow modeling, see Piran (2004).

The hydrodynamics of a GRB afterglow are typically modeled either using a semi-analytic solution for an expanding spherical blastwave, or with direct hydrodynamical fluid simulations. Since a GRB is typically only detected if the Earth is within the jet opening angle, and the outflow is initially highly relativistic, a natural model is a spherical, ultra-relativistic Blandford-McKee blastwave (Blandford & McKee 1976), as in, e.g., Granot et al. (1999); van Eerten & Wijers (2009). More accurate semi-analytic models of spherical and on-axis jet afterglows have also been used, such as an interpolation between a Blandford-McKee and Sedov-Taylor solution in DeColle et al. (2012a), and an analytic fit to 1D hydrodynamic simulations in Leventis et al. (2012).

Semi-analytic models for an off-axis observer are also possible, Granot et al. (e.g. 2002); Waxman (e.g. 2004); Rossi et al. (e.g. 2004); Morsany et al. (e.g. 2007); van Eerten et al. (e.g. 2010), but these models all assume an ultra-relativistic Blandford-McKee blastwave. Hydrodynamical simulations of on- and off-axis GRB afterglows have been carried out, Granot et al. (e.g. 2002); Cannizzo et al. (e.g. 2004); van Eerten et al. (e.g. 2010); van Eerten & MacFadyen (e.g. 2011); DeColle et al. (e.g. 2012a); De Colle et al. (e.g. 2012b). Although very accurate, full hydrodynamic simulations are computa-

tionally expensive and can only be used to directly model a small number of cases.

Our modeling approach, described in section 2, is to use a semi-analytic off-axis blastwave model that smoothly transitions between an ultra-relativistic and non-relativistic expansion, following DeColle et al. (2012a). Such a semi-analytic model is needed, rather than an analytic fit or re-scaling of previous results, because the peak flux occurs when the blastwave is mildly relativistic (Lorentz factor ~ 2) and, at low frequencies, transitioning from optically thick to optically thin.

In section 3 we use our afterglow code to make specific predictions for possible afterglow light curves of GW150914, given a range of possible model parameters. In section 4 we discuss under what conditions an afterglow of GW150914 might be detectable.

2. METHODS

We carry out modeling of the afterglow using the Trans-Relativistic Afterglow Code (TRAC). TRAC is able to solve a semi-analytic model of the emission of a relativistic fireball with an arbitrary angular distribution of energy and at an arbitrary observer angle (i.e. relative to a jet axis). TRAC is based on the methodology of Granot et al. (1999) and began development for use in Morsany et al. (2009). A full description of TRAC will be published in Morsany et al. (in prep.).

Beginning with an energy distribution and observer angle, at a given observer time, TRAC first calculates the size of the blastwave seen by the observer, along with the values of density, pressure, and Lorentz factor inside this shell. TRAC treats the evolution along each radial direction from the center of the blast as an independently evolving portion of a spherical blastwave (no transverse mixing). The semi-analytic blastwave model we use, based on the interpolation of DeColle et al. (2012a) (eqn. 1), smoothly transitions between the ultra-relativistic Blandford-McKee phase (Blandford & McKee 1976) and the non-relativistic Sedov-Taylor phase. This is particularly important for radio observations, which typically peak during the mildly relativistic transition phase. At any time, the total energy of a spherical blastwave satisfies

$$E = R^{3-k} \beta^2 \Gamma^2 \rho_0 c^2 \left[\frac{8\pi}{17-4k} \beta^2 + \frac{(5-k)^2}{4\alpha_k} (1-\beta^2) \right] \quad (1)$$

where E is the blast energy, R is the shock radius, Γ is the Lorentz factor of the shock, β is the shock velocity over c , and, for a constant density external medium, ρ_0 is the external mass density and $k = 0$.

Using the 3-dimensional grid of fluid values, TRAC then computes the integrated emission from the blastwave as a function of frequency. For the current version of TRAC, we assume the emission is due to synchrotron

radiation parameterized by ϵ_e , the fraction of energy in electrons, ϵ_B , the fraction of energy in the magnetic field, and p , the spectral index of the electron energy distribution. TRAC solves the full radiative transfer equation including synchrotron cooling and synchrotron self-absorption.

For the models presented here, we assume the shocked gas has an adiabatic index of $\gamma_{ad} = 4/3$ and that the structure behind the shock front follows that of a relativistic shock, i.e.

$$\rho(\chi) = \rho_f \chi^{-(7-2k)/(4-k)} \quad (2)$$

$$P(\chi) = P_f \chi^{-(17-4k)/(12-3k)} \quad (3)$$

$$\gamma(\chi) = \sqrt{(\gamma_f - 1)^2/\chi + 1} \quad (4)$$

where $\chi = 1 + 4(m+1)(1-r/R)\gamma_f^2$ is a self-similarity variable, ρ_f , P_f , and γ_f are density, pressure, and Lorentz factor of fluid immediately behind the shock front, and r is radius at any position behind the shock. For an impulsive explosion with $k = 0$, $m = 3$. These approximations will break down in the non-relativistic limit, introducing some error into our modeled luminosities at very late times.

For all of our afterglow models, we assume the event is located at $D = 410$ Mpc, with $\epsilon_e = 0.1$, $\epsilon_B = 0.01$, $p = 2.5$ the observer-directed kinetic energy is $E_{iso} = 1.8 \times 10^{49}$ erg, and the blastwave is expanding into a constant density environment (ISM). We use typical values for the density around observed short GRBs of $n_H = 10^{-2}$, 10^{-1} , and 10^0 cm $^{-3}$ (Fong et al. 2015).

3. RESULTS

We model the possible afterglow of GW150914 with two different basic assumptions: 1) that GW150914-GBM is an under-luminous short GRB that is isotropic or seen on-axis, or 2) that it is a typical short-GRB seen far off-axis, outside the prompt emission cone of the main jet, but with an isotropic component that accounts for the *Fermi* GBM detection. For each of these assumption, we model the afterglow with different ISM densities, and, for the off-axis models, different observer angles and jet energies. A full list of model parameters is given in table 1.

3.1. On-axis, under-luminous short GRB

For our first set of models, we assume GW150914-GBM is an under-luminous short GRB. We assume the GRB is either a beamed jet seen on-axis ($\Theta_{obs} = 0$) with a half-opening angle of $\theta_j = 10$ degrees, or is an isotropic explosion ($\theta_j = 90$ degrees). We model each case with 3 different background densities of $n_H = 10^{-2}$, 10^{-1} , and 10^0 cm $^{-3}$.

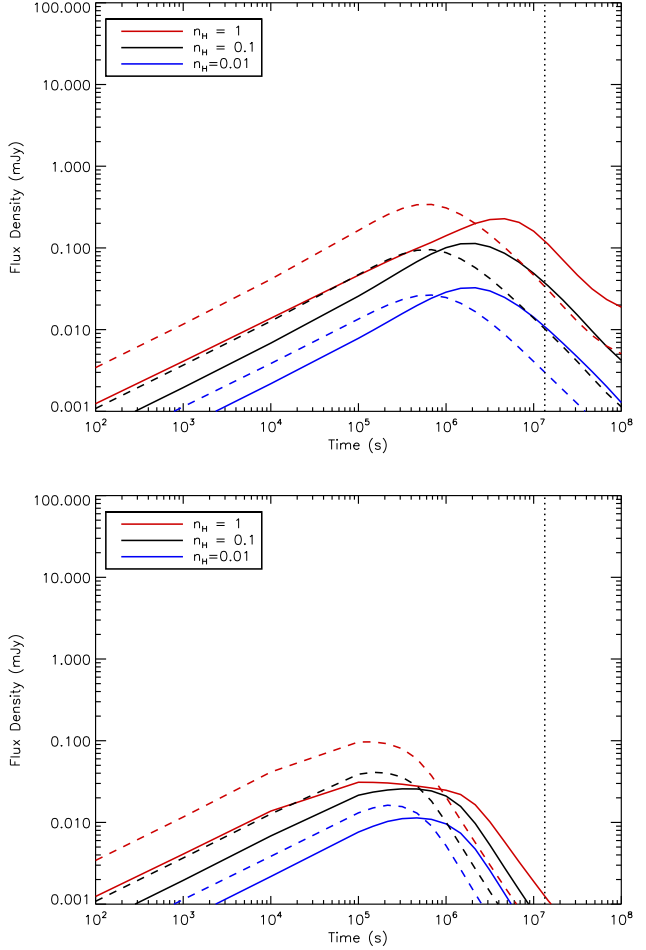


Figure 1. *Top:* Modeled afterglow flux assuming an isotropic energy distribution of 1.8×10^{49} erg at 150 MHz (solid lines) and 863.5 MHz (dashed lines). Models are for external densities of $n_H = 1$ cm $^{-3}$ (red), 0.1 cm $^{-3}$ (black) and 0.01 cm $^{-3}$ (blue). Dotted vertical line is set 5 months after the initial event, corresponding to February 17, 2016 for GW150914, the date this paper was submitted. *Bottom:* Same as top panel, but assuming the energy is in jet with $\theta_j = 10$ degrees, with $E_{iso} = 1.8 \times 10^{49}$ erg and directed towards Earth.

Fig. 1 (top panel) plots the flux predicted at Earth at 150 MHz (solid lines) and 863.5 MHz (dashed lines) for the isotropic cases. For GW150914, the vertical dotted line corresponds February 17, 2016, the submission date of this paper. Higher external density produces a brighter radio flux. It does not change the time of the peak flux, except for the highest density model at 150 MHz, where the blastwave is still optically thick. In this case the peak is delayed from 2 weeks after the GRB to 7 weeks.

In the jetted cases (fig. 1, bottom panel), higher densities lead to a slightly earlier time of peak emission, as the blastwave decelerates faster and the edge of the jet becomes visible at an earlier time (the jet break). The highest density model is again impacted by opacity at

Table 1. Model Data

| Model | E_{iso} (erg) | n_H (cm^{-3}) | Θ_{obs} (deg) | Peak flux ^a (mJy) | Peak time ^a (weeks) | Peak flux ^b (mJy) | Peak time ^a (weeks) |
|------------|--------------------|-------------------------------|-------------------------|---------------------------------|-----------------------------------|---------------------------------|-----------------------------------|
| iso | 1.8e49 | 0.1 | 0 | 0.11 | 3 | 0.10 | 1 |
| iso hi | 1.8e49 | 1 | 0 | 0.23 | 7 | 0.34 | 1 |
| iso lo | 1.8e49 | 0.01 | 0 | 0.03 | 3 | 0.03 | 1 |
| on-axis | 1.8e49 | 0.1 | 0 | 0.03 | 0.5 | 0.10 | 0.2 |
| on-axis hi | 1.8e49 | 1 | 0 | 0.03 | 0.2 | 0.04 | 0.2 |
| on-axis lo | 1.8e49 | 0.01 | 0 | 0.01 | 0.7 | 0.02 | 0.3 |
| 51.-1.30 | 1.e51 | 0.1 | 30 | 0.98 | 15 | 0.80 | 7 |
| 51.-1.20 | 1.e51 | 0.1 | 20 | 1.45 | 10 | 1.61 | 5 |
| 51.-1.40 | 1.e51 | 0.1 | 40 | 0.64 | 20 | 0.39 | 15 |
| 51.0.30 | 1.e51 | 1 | 30 | 1.17 | 20 | 3.11 | 5 |
| 51.-2.30 | 1.e51 | 0.01 | 30 | 0.30 | 20 | 0.17 | 15 |
| 51.0.20 | 1.e51 | 1 | 20 | 1.22 | 15 | 5.14 | 3 |
| 52.-1.30 | 1.e52 | 0.1 | 30 | 7.3 | 30 | 7.6 | 15 |
| 52.0.30 | 1.e52 | 1 | 30 | 6.8 | 50 | 25.6 | 10 |
| 52.-1.20 | 1.e52 | 0.1 | 20 | 10.6 | 20 | 15.5 | 10 |
| 52.0.20 | 1.e52 | 1 | 20 | 6.8 | 50 | 42.3 | 7 |

^aat 150 MHz^bat 863.5 MHz

150 MHz, limiting its peak flux density to 0.03 mJy and placing the apparent peak time at about 1 day.

All on-axis and isotropic cases produce a low flux, reaching at most 0.23 mJy at 150 MHz and 0.34 mJy at 863.5 MHz for the spherical high-density model at about 50 days after the LIGO event. This would be a very difficult detection for any low-frequency radio array due to source confusion (Tingay et al. 2013).

3.2. Off-axis normal short GRB

Next, we model the afterglow as arising from an off-axis short GRB with a range typical short GRB parameters. In all cases, we assume a jet with a half-opening angle of $\theta_j = 10$ degrees, consistent with short GRB observations (Fong et al. 2015). LIGO loosely constrains the inclination of the orbital plane of the binary black holes in GW150914, with the most likely value being an inclination of ~ 150 degrees (LIGO 2016). Assuming the jet axis is aligned with the binary orbital plane, this would place the jet axis ~ 30 degrees away from our line of sight ($\Theta_{obs} = 30$ degrees). We model observer angles of 20, 30, and 40 degrees to cover a range of possible values. We also model a range of external densities ($n_H = 10^{-2}, 10^{-1}$ and 10^0 cm^{-3}) and isotropic energies within the jet to $E_{iso} = 10^{51}$ or 10^{52} erg. All off-axis models have an isotropic component with an energy of 1.8×10^{49} erg.

Fig. 2 (top panel) shows our models for a 10^{51} erg jet 30 degrees off axis, with 3 different external densities

at 150 MHz (solid lines) and 863.5 GHz (dashed lines). The initial evolution follows the isotropic model cases (see fig. 1). However, after 3 days to 3 weeks, the jet decelerates sufficiently that it begins to become visible to an off-axis observer. High external densities decelerate the jet faster, producing an earlier and brighter peak flux. For an external density of $n_H = 1 \text{ cm}^{-3}$, the jet is still self-absorbed at 150 MHz when it comes into view, reducing the peak flux and delaying the observed peak until 6 months vs. 1 month at 863.5 MHz. The self-absorbed case will also have a hard spectrum (slope of ~ 1.6), while the other case have a soft spectrum (slope of ~ 0) at 150 MHz. The $n_H = 0.1$ and 1 cm^{-3} models each reach a peak flux density of about 1 mJy 4 to 6 months after the GRB. All three cases would be easily detectable by ATCA at higher frequencies with a good localization.

Fig. 2 (bottom panel) shows the results of varying the observer angle for models with $E_{iso} = 10^{51}$ erg and an $n_H = 0.1 \text{ cm}^{-3}$. Moving closer to the jet axis increase the observed peak flux and moves the peak earlier in time, from about 2 months to 3 months to 5 months at 863.5 MHz for $\Theta_{obs} = 20, 30$, and 40 degrees, respectively. At late times, once the entire jet is in view, the declining flux is nearly identical regardless of observer angle.

If the jet energy is $E_{iso} = 10^{52}$ erg, fig. 3 (top panel), the peak time moves later by a factor of two and the peak flux increases a factor of about 7 relative to mod-

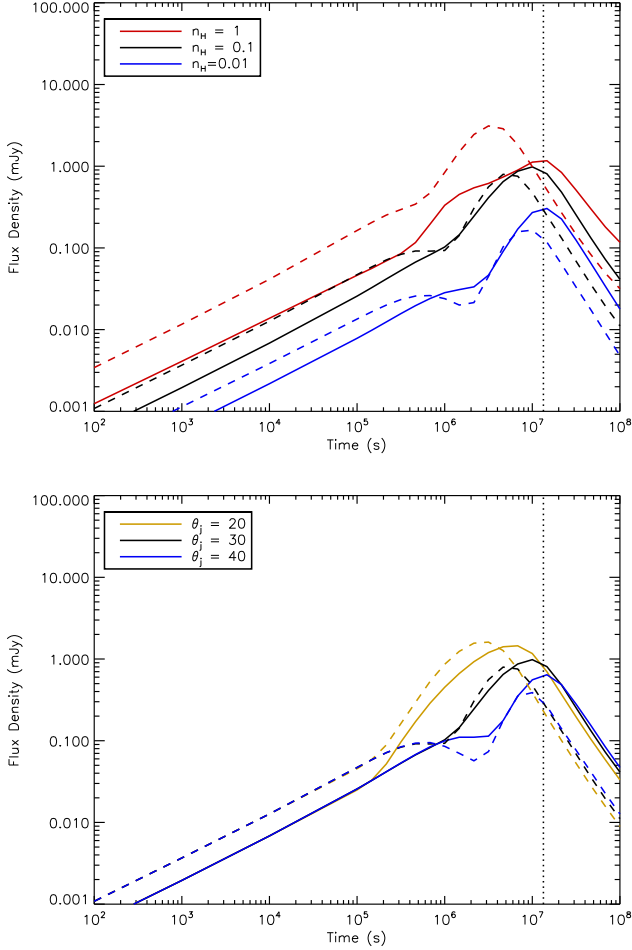


Figure 2. *Top:* Same as fig. 1, but assuming an off-axis jet with $E_{iso} = 10^{51}$ erg in addition to the isotropic component, with the observer at $\Theta_{obs} = 30$ degrees. *Bottom:* Same as top panel, but assuming an external density of $n_H = 0.1 \text{ cm}^{-3}$ for all models, and an observer angle of $\Theta_{obs} = 20$ (orange), 30 (black), and 40 (blue) degrees.

els with $E_{iso} = 10^{51}$ erg. With a peak flux density $\geq 7 \text{ mJy}$ at 150 MHz 6 to 12 months after GW150914, a GRB with these parameters would be detectable with the MWA now, and may continue to brighten for next several months (after the vertical dotted line). The 863.5 MHz flux density is up to 10's of mJy and should be detectable by ASKAP. It would also be easily detectable by the ATCA given an afterglow candidate or sufficiently small search region.

At low frequencies the flux peak occurs near the time when the jet is becoming optically thin. This leads to a large change in spectral slope near the peak, as seen in fig. 3 (bottom panel). The spectra just before the peak flux is reached becomes as hard as $F_\nu \propto \nu^{-2}$ in the high density case ($F_\nu \propto \nu^{-1}$ at medium density) before decreasing and ultimately falling to $F_\nu \propto \nu^{-0.75}$ at late times. At higher frequencies the jet becomes optically thin before the peak is reached, creating a less dramatic

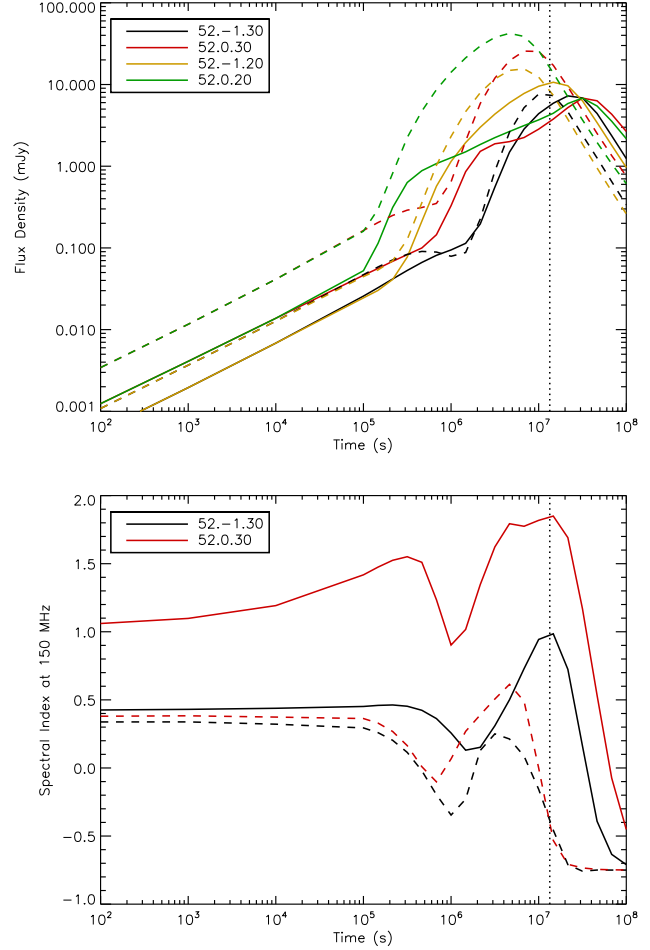


Figure 3. *Top:* Same as fig. 2, but showing afterglow models for $E_{iso} = 10^{52}$ erg for $\Theta_{obs} = 30$ degrees with external densities of $n_H = 0.1 \text{ cm}^{-3}$ (black) and 1 cm^{-3} (red), and $\Theta_{obs} = 20$ degrees with external densities of $n_H = 0.1 \text{ cm}^{-3}$ (orange) and 1 cm^{-3} (green). Names in legends correspond to table 1. *Bottom:* The spectral slope of radio emission averaged between 80 and 300 MHz (solid lines) and between 713.5 and 1013.5 MHz (dashed lines) for models with $E_{iso} = 10^{52}$ erg, $\Theta_{obs} = 30$ degrees and external densities of $n_H = 0.1 \text{ cm}^{-3}$ (black) and 1 cm^{-3} (red). Dotted vertical lines are set 5 months after the initial event, corresponding to February 17, 2016 for GW150914, the date this paper was submitted.

change in slope, from about $F_\nu \propto \nu^{-1/3}$ before the peak to $F_\nu \propto \nu^{-0.75}$ at late times. The change in spectral slope from hard to soft, particularly at low frequencies, could be used to find promising afterglow candidates for GW150914.

3.3. X-ray and Radio Afterglow

The modeled R-band optical afterglow of select models are shown in fig. 4 (top panel). At early times, before the relativistic outflow has decelerated significantly, the afterglow is dominated by the Earth-directed energy. Optical emission initially peaks at 100s at about magnitude 18.1 (19.4) for an external density of 1 (0.1) cm^{-3}

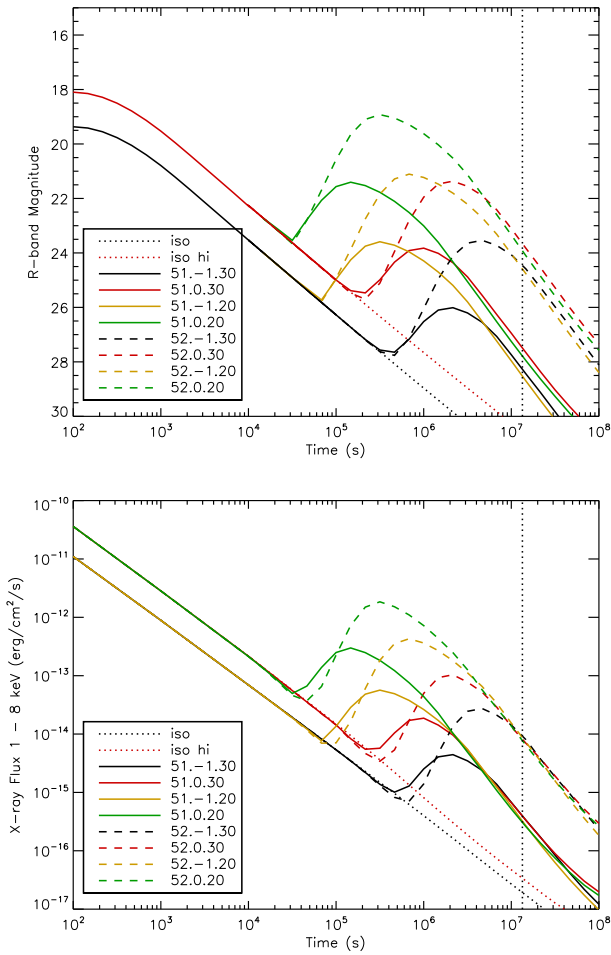


Figure 4. *Top:* Modeled afterglow R-band magnitude for selected models. *Bottom:* Modeled afterglow X-ray flux integrated from 1 - 8 keV for selected models. Names in legends correspond to table 1.

and then rapidly fades.

For the off axis-models, there is a second peak when the jet comes into view. This peak is only brighter than 22nd magnitude for the most optimistic model parameters, e.g. a combination of high external density, high E_{iso} , and small observer angle. However, under such favorable circumstances the afterglow of GW150914-GRB would have been detectable by Pan-STARRS at several days to months after the LIGO detection, if it was in Pan-STARRS field of view. The late time optical luminosity is set by the energy of the jet, and at the present even the most optimistic models would be 24th magnitude. Our optical modeling does not include potential contributions from a non-relativistic supernova or kilonova counterpart.

In the X-ray (fig. 4, bottom panel), the afterglow is as bright as 3.6×10^{-11} erg cm $^{-2}$ s $^{-1}$ between 1 and 8 keV and is still brighter than 10^{-15} erg cm $^{-2}$ s $^{-1}$ at 1 day in all models. For the off-axis models, the X-rays re-

brighten to above 8×10^{-16} erg cm $^{-2}$ s $^{-1}$, and to as much as 2×10^{-12} erg cm $^{-2}$ s $^{-1}$ in the brightest case. This is below the detection limit of *Swift* LMC observations over a portion of the error box of GW150914 (Evans et al. 2016).

At late times, the X-ray flux is mostly set by the E_{iso} of the jet. At the present time, the X-ray afterglow would be about 3×10^{-16} erg cm $^{-2}$ s $^{-1}$ for $E_{iso} = 10^{51}$ erg and 7×10^{-15} erg cm $^{-2}$ s $^{-1}$ for $E_{iso} = 10^{52}$ erg. If GW150914 were localized, an afterglow this bright would still be detectable by *Chandra* or *XXM* observations.

4. CONCLUSIONS

If GW150914-GBM is associated with the LIGO detection of GW150914, and assuming it is an off-axis short GRB with a relatively bright jet ($E_{iso} = 10^{52}$ erg), its afterglow would be detectable **NOW** at 150 MHz with, e.g., the MWA (see fig 3) and at 863.5 MHz with ASKAP. Under these conditions, if an afterglow candidate were found, it would be easily observable at higher radio frequencies by the ATCA (~ 10 mJy at 1.4GHz), in X-rays by *Chandra* or *XXM* ($\sim 10^{-14}$ erg cm $^{-2}$ s $^{-1}$), and possibly with deep optical followup (~ 24 th mag. in R-band).

If GW150914-GBM has a more typical short GRB energy of $E_{iso} = 10^{51}$ erg, it would likely not be detectable by the MWA, reaching a peak flux density of at most 1 mJy at 150 MHz. It may still be detectable with ASKAP at 863.5 MHz, where the peak flux density is as high as 5 mJy. However, if an afterglow candidate or sufficiently small error box were identified such an afterglow would be observable by the ATCA (> 0.1 mJy at 1.4 GHz for all models) and possibly deep X-ray observations ($\sim 3 \times 10^{-16}$ erg cm $^{-2}$ s $^{-1}$) at the present time.

If instead GW150914-GBM is a very low luminosity short GRB, either isotropic or beamed, with $E_{iso} = 1.8 \times 10^{49}$ erg, it was likely never bright enough to be observable without an immediate localization. Only the higher frequency radio flux would be potentially detectable after the first few hours, at ~ 0.3 mJy for a dense external medium.

Given the high rates of black hole mergers inferred from the LIGO detection of GW150914 (Abbott et al. 2016b), if such events do produce short GRBs, future events with slightly more favorable properties should be observable. Having a large GRB jet energy, high external density, jet axis closer to our line of sight, closer distance to Earth, or better initial localization would all favor the detection of an associated relativistic afterglow with follow-up radio, optical, and X-ray searches.

ACKNOWLEDGMENTS

BJM was supported by an NSF Astronomy and Astrophysics Postdoctoral Fellowship under grant AST1102796, by the Aspen Center for Physics under

NSF grant PHY-1066293, and by the NSF under grant AST1333514. Dominic Ryan was supported as an REU student under NSF grant AST1004881.

REFERENCES

Abbott, B. P., Abbott, R., Abbott, T. D., et al. 2016, *Phys. Rev. Lett.*, 116, 061102

Abbott, B. P., Abbott, R., Abbott, T. D., et al. 2016, ArXiv e-prints, arXiv:1602.03842

Bannister, K., et al. 2015, *GCN Circ.* 18363, <http://gcn.gsfc.nasa.gov/gcn3/18363.gcn3>

Blandford, R. D., & McKee, C. F. 1976, *Physics of Fluids*, 19, 1130

Cannizzo, J. K., Gehrels, N., & Vishniac, E. T. 2004, *ApJ*, 601, 380

Connaughton, V., Burns, E., Goldstein, A., et al. 2016, ArXiv e-prints, arXiv:1602.03920

De Colle, F., Granot, J., López-Cámarra, D., & Ramirez-Ruiz, E. 2012, *ApJ*, 746, 122

De Colle, F., Ramirez-Ruiz, E., Granot, J., & López-Cámarra, D. 2012, *ApJ*, 751, 57

Evans, P. A., Kennea, J. A., Barthelmy, S. D., et al. 2016, ArXiv e-prints, arXiv:1602.03868

Fong, W., Berger, E., Margutti, R., & Zauderer, B. A. 2015, *ApJ*, 815, 102

Granot, J., Panaiteescu, A., Kumar, P., & Woosley, S. E. 2002, *ApJL*, 570, L61

Granot, J., Piran, T., & Sari, R. 1999, *ApJ*, 527, 236

Hobbs, G., Heywood, I., Bell, M. E., et al. 2016, *MNRAS*, 456, 3948

Leventis, K., van Eerten, H. J., Meliani, Z., & Wijers, R. A. M. J. 2012, *MNRAS*, 427, 1329

Li, X., Zhang, F.-W., Yuan, Q., et al. 2016, ArXiv e-prints, arXiv:1602.04460

Morsony, B. J., Lazzati, D., & Begelman, M. C. 2007, *ApJ*, 665, 569

Morsony, B. J., Workman, J. C., Lazzati, D., & Medvedev, M. V. 2009, *MNRAS*, 392, 1397

Piran, T. 2004, *Reviews of Modern Physics*, 76, 1143

Rossi, E. M., Lazzati, D., Salmonson, J. D., & Ghisellini, G. 2004, *MNRAS*, 354, 86

Savchenko, V., Ferrigno, C., Mereghetti, S., et al. 2016, ArXiv e-prints, arXiv:1602.04180

Smartt, S. J., Chambers, K. C., Smith, K. W., et al. 2016, ArXiv e-prints, arXiv:1602.04156

Soares-Santos, M., Kessler, R., Berger, E., et al. 2016, ArXiv e-prints, arXiv:1602.04198

The LIGO Scientific Collaboration, & the Virgo Collaboration. 2016, ArXiv e-prints, arXiv:1602.03840

Tingay, S. J., Goeke, R., Bowman, J. D., et al. 2013, *PASA*, 30, e007

van Eerten, H., Zhang, W., & MacFadyen, A. 2010, *ApJ*, 722, 235

van Eerten, H. J., & MacFadyen, A. I. 2011, *ApJL*, 733, L37

van Eerten, H. J., & Wijers, R. A. M. J. 2009, *MNRAS*, 394, 2164

Wanderman, D., & Piran, T. 2015, *MNRAS*, 448, 3026

Waxman, E. 2004, *ApJ*, 602, 886